The Astrophysical Journal, 824:87 (11pp), 2016 June 20 doi:10.3847/0004-637X/824/2/87

LONG-TERM STUDY OF THE DOUBLE PULSAR J0737–3039 WITH *XMM-NEWTON*: PULSAR TIMING

M. N. Iacolina[1], A. Pellizzoni[1], E. Egron[1], A. Possenti[1], R. Breton[2], M. Lyutikov[3], M. Kramer[2,4], M. Burgay[1], S. E. Motta[5], A. De Luca[6], and A. Tiengo[6,7,8]
[1] INAF—Osservatorio Astronomico di Cagliari, Via della Scienza 5, I-09047—Selargius (CA), Italy; iacolina@oa-cagliari.inaf.it
[2] Jodrell Bank Centre for Astrophysics, The University of Manchester, Manchester, M13 9PL, UK
[3] Department of Physics, Purdue University, 525 Northwestern Avenue, West Lafayette, IN 47907-2036, USA
[4] Max-Planck-Institut für Radioastronomie, Auf dem Hügel 69, D-53121 Bonn, Germany
[5] University of Oxford—Department of Physics, Astrophysics—Keble Road, Oxford OX1 3RH, UK
[6] INAF—Istituto di Astrofisica Spaziale e Fisica Cosmica Milano, Via E. Bassini 15, I-20133 Milano, Italy
[7] Istituto Universitario di Studi Superiori, Piazza della Vittoria 15, I-27100, Pavia, Italy
[8] INFN, Sezione di Pavia, via A. Bassi 6, I-27100, Pavia, Italy
Received 2015 April 15; accepted 2016 January 5; published 2016 June 16

ABSTRACT

The relativistic double neutron star binary PSR J0737−3039 shows clear evidence of orbital phase-dependent wind-companion interaction, both in radio and X-rays. In this paper, we present the results of timing analysis of PSR J0737−3039 performed during 2006 and 2011 *XMM-Newton* Large Programs that collected ∼20,000 X-ray counts from the system. We detected pulsations from PSR J0737−3039A (PSR A) through the most accurate timing measurement obtained by *XMM-Newton* so far, the spin period error being of 2×10^{-13} s. PSR A's pulse profile in X-rays is very stable despite significant relativistic spin precession that occurred within the time span of observations. This yields a constraint on the misalignment between the spin axis and the orbital momentum axis $\delta_A \approx 6.6^{+1.3}_{-5.4}$ deg, consistent with estimates based on radio data. We confirmed pulsed emission from PSR J0737−3039B (PSR B) in X-rays even after its disappearance in radio. The unusual phenomenology of PSR B's X-ray emission includes orbital pulsed flux and profile variations as well as a loss of pulsar phase coherence on timescales of years. We hypothesize that this is due to the interaction of PSR A's wind with PSR B's magnetosphere and the orbital-dependent penetration of the wind plasma onto PSR B closed field lines. Finally, the analysis of the full *XMM-Newton* data set provided evidence of orbital flux variability (∼7%) for the first time, involving a bow-shock scenario between PSR A's wind and PSR B's magnetosphere.

Key words: binaries: general – pulsars: general – pulsars: individual (PSR J0737–3039A, PSR J0737–3039B) – stars: neutron – X-rays: stars

1. INTRODUCTION

PSR J0737−3039 (Burgay et al. 2003; Lyne et al. 2004) is still the most interesting binary system allowing studies on plasma physics, general relativity, and matter in the strong-field regime (Kramer et al. 2006; Kramer & Wex 2009). This is the only known double neutron star system in which both neutron stars have been detected as pulsars. Its orbital period is 2.4 hr, and it contains a mildly recycled pulsar with a spin period of 22.7 ms (PSR J0737−3039A—hereafter PSR A), and a 2.77 s pulsar (PSR J0737−3039B—hereafter PSR B).

The uniqueness of this system is derived from its highly relativistic nature and from the presence of the two interacting pulsars separated by only ∼3 light-seconds whose orbital plane is observed nearly edge-on ($i \approx 88.^\circ7$; Ransom et al. 2004). This has allowed astronomers and theoretical physicists to undertake different kinds of studies never carried out before and to obtain new proven results on many lines of researches. The works of Burgay et al. (2003) and Kalogera et al. (2004) led to an upward estimate of the coalescence rate of neutron star binaries. The angle between the PSR A's spin axis and the orbital angular momentum was constrained to a small value ($\delta \lesssim 4.^\circ7$) by Manchester et al. (2005) and Ferdman et al. (2013). Furthermore, while McLaughlin et al. (2004c) discovered a strong modulation of pulsed flux density of PSR A with the periodicity of PSR B during PSR A's radio eclipse (when it passes behind PSR B), the studies of Breton et al. (2008) allowed us to measure PSR B's spin-orbit precession. Perera et al. (2010) presented the evolution of PSR B's radio emission, providing an update to Burgay et al. (2005) by describing the changes in the pulse profile and flux density over five years of observations, culminating in PSR B's radio disappearance in 2008 March. Over this time, the pulse profile evolved from a single to a double peak, most likely due to relativistic spin precession coupled with an elliptical beam. In this context, PSR B's radio reappearance is expected to happen at the earliest in ∼2035 with the same part of the beam —if we assume a symmetric bipolar beam shape, we should have detected PSR B in ∼2014—(Perera et al. 2010; Lomiashvili & Lyutikov 2014). However, the observed decrease in flux over time and PSR B's disappearance is difficult to explain using current models and may be due to the changing influence of PSR A on PSR B. For a comprehensive review of the most interesting scientific results obtained from the study of the Double Pulsar in the radio band so far, see, e.g., Kramer & Stairs (2008) and Kramer & Wex (2009).

High-energy (X-ray and γ-ray) observations provide a fundamental complement to radio studies for what concerns the physics of the magnetospheric and surface emissions and mutual interactions in the close environment of the two neutron stars (Campana et al. 2004; McLaughlin et al. 2004a; Pellizzoni et al. 2004; Chatterjee et al. 2007; Pellizzoni et al. 2008; Possenti et al. 2008; Guillemot et al. 2013). High-energy studies of PSR J0737−3039 could, for example, reveal an intra-binary shock caused by the relativistic particle wind coming from PSR A and impacting the magnetosphere of PSR B (Lyutikov 2004). Furthermore, it is possible to obtain

information on the peculiar magnetospheric emission mechanisms of the two close orbiting neutron stars. In particular, detection and monitoring of PSR B in X-rays is of paramount importance after its disappearance in the radio band, providing a unique way to keep monitoring and roughly timing this neutron star.

Pellizzoni et al. (2008) reported the results of a ∼230 ks long X-ray observation of PSR J0737−3039 obtained within the framework of *XMM-Newton* "Large Programs" in 2006 October. The analysis of ∼5600 source photons obtained from this observation confirmed the detection of pulsed X-ray emission from PSR A (originally revealed by *Chandra*; Chatterjee et al. 2007). PSR A shows peculiar properties with respect to other known recycled pulsars (e.g., the softest nonthermal spectrum) possibly due to the particular evolutionary history of a double neutron star system.

For the first time, X-ray pulsed emission from PSR B was also detected with good confidence (∼200–300 pulsed counts) around the ascending node of the orbit, though poorly constrained in terms of flux, light-curve shape, and spectrum. Due to its low rotational energy loss (PSR B spin-down energy is $\dot{E}_{\rm PSR\,B} = 4\pi^2 I \dot{P} P^3 \simeq 1.7 \times 10^{30}\,{\rm erg\,s^{-1}}$, with I the moment of inertia of the neutron star, P the spin period, and $\dot{P}$ its derivative), X-ray emission from PSR B can only be powered by an external source, i.e., the spin-down energy from PSR A ($\dot{E}_{\rm PSR\,A} \simeq 6 \times 10^{33}\,{\rm erg\,s^{-1}}$) impacting PSR B's magnetosphere. In this scenario, it was estimated that ∼2% of the rotational energy loss from PSR A is converted into (possibly thermal) radiation from PSR B. The actual energy transfer and emission mechanisms are still a matter of debate (Zhang & Loeb 2004; Lyutikov 2005; Lyutikov & Thompson 2005; Breton et al. 2012).

Pellizzoni et al. (2008) found no signs (e.g., orbital flux modulation and/or a significant nonthermal component in PSR A's off-pulse) of the presence of X-ray emission from a bow-shock between PSR A's wind and PSR B's magnetosphere invoked in various models (e.g., Lyutikov 2004; Arons et al. 2005) to explain the occultation of radio emission of PSR A at the inferior conjunction of PSR B. The upper limit on the flux of such a shock component constrains the wind magnetization parameter $\sigma_{\rm M}$ of PSR A to values >1, much higher than that predicted by the radio occultation of PSR A due to the presence of a magnetosheath (the shocked layer of PSR A's wind at PSR B's magnetosphere). The absorption causing PSR A's occultation occurs within PSR B's magnetosphere, which retains enough plasma to produce an eclipse (Lyutikov & Thompson 2005; Breton et al. 2008, 2012).

In order to shed light and deepen the above scenarios, and to monitor the system evolution in X-ray on a timescale of years, a new ∼360 ks *XMM-Newton* observation was performed in 2011 October. In this paper, we present the overall timing analysis results of the full ∼590 ks *XMM-Newton* data set on PSR J0737−3039 including both 2011 and 2006 observations. Spectral analysis results are instead reported by E. Egron et al. (2016, in preparation).

2. OBSERVATIONS AND DATA REDUCTION

Our work initially focused on the most recent *XMM-Newton* observation of PSR J0737−3039 performed in 2011 October. The Double Pulsar was observed for three consecutive *XMM-Newton* orbits, whose lengths and start times are indicated in Table 1, where details of observations are summarized. The total time span of the observation covered ∼41 binary orbits (363.7 ks). Data were obtained with the European Photon Imaging Camera (EPIC): two *EPIC-MOS* detectors (each made up of an array of 7 CCDs; Turner et al. 2001) and one *EPIC-pn* camera (an array of 12 CCDs; Strüder et al. 2001), operating in Small-Window mode (with thin optical filter), a $2' \times 2'$ field of view in the central CCD with a time resolution of 0.3 s for the *EPIC-MOS* cameras, and a $4' \times 4'$ field of view with a 5.67 ms time resolution for the *EPIC-pn* camera.[9]

Table 1
XMM-Newton Observations of PSR J0737−3039 for the 2011 Large Program[a]

Orbit ID	Start Date	*EPIC* Detector	Total Source Counts[b]	Background Fraction[c] (%)	Exposure[d] (ks)
2174	2011 Oct 22	*pn*	3165	31.2	88
		MOS1	582	10.0	104
		MOS2	686	14.4	122
2175	2011 Oct 24	*pn*	2987	40.1	65
		MOS1	724	22.5	84
		MOS2	713	22.1	84
2176	2011 Oct 26	*pn*	2603	21.3	83
		MOS1	746	11.6	112
		MOS2	733	17.0	112

Notes.
[a] For the 2006 observation, see Table 1 in Pellizzoni et al. (2008).
[b] Total counts in the source extraction region.
[c] Percentage of the background on the on-source total counts.
[d] Total good time after dead-time correction and soft proton flare screening.

Data analysis has been performed using the *XMM-Newton* Science Analysis Software (SAS), version 11.0.0. The first step was to process data with `emproc` and `epproc`, standard pipeline tasks for *EPIC-MOS* and *EPIC-pn* observations respectively. In order to reduce the background contamination, we selected data with photon pattern 0–12 for the *EPIC-MOS* while, for the *EPIC-pn*, pattern 0–4 for energies higher than 0.4 keV and 0 for energies lower than 0.4 keV. Part of the data was affected by background flares. We excluded such episodes by extracting a 10 s time binned light curve in the 0.15–10 keV energy range from the whole field of view for each camera, omitting the source region, and selecting events below a threshold of 5σ of the quiescent rate for the *EPIC-pn* and 3σ for the *EPIC-MOS*.

The radius of the source extraction region was set to 18″ for the *EPIC-pn* and 15″ for the *EPIC-MOS* data. After testing a range of thresholds for the background, different photon pattern selections, and source extraction radii, the adopted background flares rejection and extraction criteria described above proved to maximize the detection significance of the light curves of PSR A and PSR B in the 0.15–10 keV energy range (see Sections 3 and 4).

The resulting good exposure times and counts statistics for the source and the background related to the 2011 observations are listed in Table 1.

Data related to the 2006 October observation and published by Pellizzoni et al. (2008) were reprocessed using the same method and tasks described above for the new 2011s data set in order to consistently and equally process the whole *XMM-*

[9] Note that *EPIC-pn* higher time-resolution modes (⩽30 μs) are only suitable for very bright sources: http://xmm.esac.esa.int/external/xmm_user_support/documenta-tion/uhb_2.1/XMM_UHB.html

Newton data set, before proceeding with the comprehensive long-term timing analysis of PSR J0737−3039. For details of the 2006 observations (∼230 ks of data) see Table 1 of Pellizzoni et al. (2008). Note that also in that case both *EPIC-MOS* detectors and *EPIC-pn* camera were operated in Small-Window mode.

In order to perform high-precision timing analysis on such a large data span, the filtered event lists have been solar system barycentered using the recent and accurate JPL DE405 Planetary Ephemeris.[10] Note that this option was not available for the SAS version 7.1.0 at the time of 2006 data reduction (implicitly using obsolete JPL DE200 Ephemeris).

The last step in the data reduction before entering timing analysis was to correct data for the effects of the relativistic orbital motion of the binary system, according to Blandford & Teukolsky (1976), with the same procedure as in Pellizzoni et al. (2008), and using the ephemerides from Kramer et al. (2006) for both PSR A and PSR B.

The *XMM-Newton* Science Operations Centre (SOC) reported that the observation of PSR J0737−3039 in revolutions 2174, 2175, and 2176 originally suffered from time stamp drifts at the Perth Ground Station, claiming possible corruption on the time dependent analysis of the data. In fact, we performed an early quick-look timing analysis providing a coarse light curve of PSR A that revealed an evident loss of signal coherence among and within different *XMM-Newton* revolutions. In 2012 January the *XMM-Newton* SOC was able to fully fix the problem regenerating the Time Correlation file and reingesting the ODFs in the archive. The timing analysis presented in the following sections refers to the last version of the ODFs (ID 0670810101/201/301, release 2) in the *XMM-Newton* public archives, apparently free from any further time stamp problems.

3. LONG-TERM X-RAY TIMING OF PSR J0737−3039A

The combination of 2006 and 2011 data sets provided ∼13,500 *EPIC-pn*[11] counts from the source region suitable for pulsar timing analysis.

We searched for a pulsar signal in a wide spin period interval centered at the value predicted by the radio ephemeris from Kramer et al. (2006; keeping all of the other ephemeris values fixed) in order to check for possible discrepancies among X-ray and radio timing solutions. We applied the bin independent Z_n^2 test statistics (Buccheri et al. 1983) to the light curves obtained by folding the data at each trial period. The adopted period search resolution was $\delta P = P^2/(T_{\rm obs} n_{\rm bin}) = 2 \times 10^{-13}$ s, where P is PSR A's spin period, $T_{\rm obs}$ is the time span of the whole observation and $n_{\rm bin}$ is the number of bins used to fold the light curve ($n_{\rm bin} = 20$ is a suitable choice given the relatively moderate *EPIC-pn* time resolution). The results are shown in Figure 1 (left panel) for a Z_n^2 test with $n = 2$ harmonics. The curve presents several peaks corresponding to different trial frequency values. It can be explained considering that the data set is not continuous, but composed of five *XMM-Newton* orbits related to different observing epochs. In particular, we have a big time gap in the data between the 2006 and 2011 Large Programs and a total of three additional gaps between the two and the three *XMM-Newton* orbits of 2006 and 2011 data respectively. This introduced some periodicities featuring the periodogram as an "interference +diffraction"-like diagram. The strongest signal, providing $Z_2^2 \sim 1200$ with an almost null probability to be obtained by chance even accounting for the over 10^4 period trials, occurred for the period $P_{\rm A,X} = 22.6993785996(2)$ ms referred to the epoch 53156.0 MJD of the radio ephemeris (the error quoted in parenthesis corresponds to the resolution of the search). This value is consistent with $P_{\rm A,radio} = 22.699378599624(1)$ ms, expected at the same epoch.

It is worth noting that PSR A's radio ephemeris from Kramer et al. (2006) is still valid several years beyond the range of the timing data (MJDs 52760–53736). This is due to the high-precision measurements of Keplerian and post-Keplerian parameters of the binary orbit, and to the high-stability of the millisecond pulsar not affected by glitches or significant timing noise.

The pulse profile corresponding to the above best timing solution is shown in Figure 1, top right panel. The background-subtracted light curve is shown for three different energy ranges: the band that maximizes the signal-to-noise ratio (0.15–3.0 keV) and two sub-bands highlighting the behavior at low (0.15–0.5 keV) and at high-energy (0.8–3.0 keV). Error bars are calculated according to the expression $\sigma_{\rm i} = (C_{\rm i} + B_{\rm i} f^2)^{1/2}$, where $C_{\rm i}$ and $B_{\rm i}$ are the total counts and the background counts for each bin of the light curve, and f is the ratio between the source and background extraction area ($f \simeq 0.1$). The pulsed counts can be estimated through the expression $\mathrm{PF} \equiv (C_{\rm tot} - n_{\rm bin} N_{\rm min})$ (and its associated error $\sigma_{\rm PF} = (C_{\rm tot} + n_{\rm bin}^2 N_{\rm min})^{1/2}$), where $C_{\rm tot}$ are the total counts and $N_{\rm min}$ are the counts from the bin of the minimum of the light curve. For the full 0.15–3.0 keV energy range the pulsed flux is $F_{\rm PSR\,A} \approx 5.1^{+1.2}_{-0.9} \times 10^{-14}$ erg cm^{-2} s^{-1} (assuming the best-fit two-component model PL+BB, as in Pellizzoni et al. 2008), corresponding to a pulsed counts fraction of 60% ± 4% ($n_{\rm bin} = 20$) with respect to the total background-subtracted source counts. Assuming a distance of $d_{\rm PSR\,A} \approx 1.1$ kpc (Verbiest et al. 2012), the luminosity of PSR A ($L_{\rm PSR\,A} = \Omega_{\rm A} d_{\rm PSR\,A}^2 F_{\rm PSR\,A}$) results in $5.9 \times 10^{29} \Omega_{\rm A}$ erg s^{-1}, with an X-ray efficiency $L_{\rm PSR\,A}/\dot{E}_{\rm PSR\,A} \sim 10^{-4}\Omega_{\rm A}$, where $\Omega_{\rm A}$ (∼1–10 steradians) is the pulsar beam solid angle, a value in agreement with the expectation for the recycled millisecond pulsar if $\Omega_{\rm A} > 1$ (Becker & Trümper 1999; Possenti et al. 2002).

The spectral hardness ratio as a function of the pulsar phase was calculated according to the expression $(H_{\rm i} - S_{\rm i})/(H_{\rm i} + S_{\rm i})$, where $H_{\rm i}$ and $S_{\rm i}$ are the counts in each bin for the hard (0.8–3.0 keV) and soft (0.15–0.3 keV) energy ranges respectively. The result is shown in Figure 1, bottom-right panel, and confirms the behavior exhibited in Pellizzoni et al. (2008), indicating a softer spectrum in correspondence to the minimum of the pulse profile. To better investigate this feature, we analyzed the pulsed emission in different energy bands. The background-subtracted light curves for four different energy bands (0.15–0.3 keV; 0.3–0.5 keV; 0.5–0.8 keV; 0.8–3.0 keV) show that the pulsed fraction increases from ∼50% to ∼70% as the energy in the intervals increases with a similar trend in 2006 and 2011.

In order to search for a possible temporal evolution of the PSR A pulse profile caused, e.g., by relativistic pulsar spin precession (having a period of ∼75 years; Lyne et al. 2004), we

[10] http://ssd.jpl.nasa.gov/?planet_eph_export

[11] The *EPIC-MOS* data cannot be used to perform PSR A timing because of the relatively poor time resolution of the instruments, over an order of magnitude higher than the pulsar spin period.

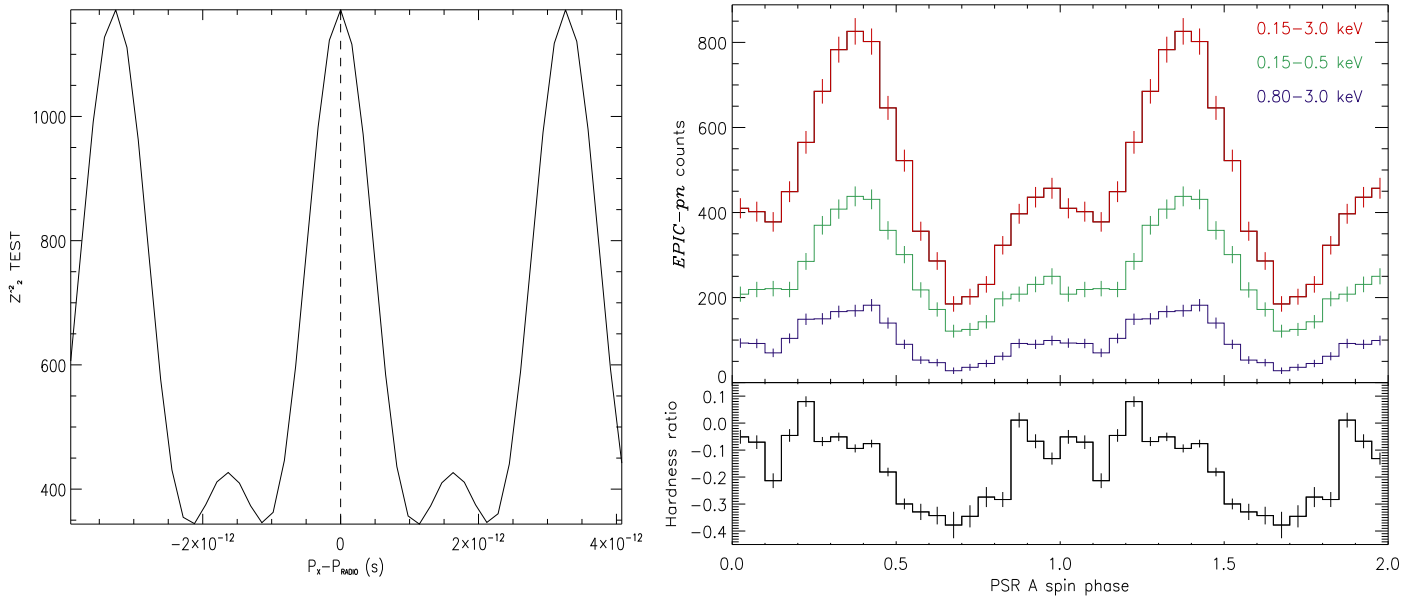

Figure 1. Left: result of the pulsar spin period search trials around PSR A's radio ephemeris solution. The most significant X-ray pulsed detection corresponds to a Z_2^2-test value of ∼1200 and is precisely aligned (within $\sim 10^{-13}$ s) with the radio period indicated by the dashed vertical line. Top right: background-subtracted light curve of PSR A for the energy band 0.15–3.0 keV (in red) and two sub-bands at low (0.15–0.5 keV, green) and high (0.8–3.0 keV, blue) energies, resulting from epoch folding of all available *EPIC-pn* data (2006+2011). Bottom right: phase-resolved hardness ratio between the hard (0.8–3.0 keV) and soft (0.15–0.3 keV) energy bands.

compared the light curve obtained in 2006 from the first *XMM-Newton* Large Program (Pellizzoni et al. 2008) to that obtained from the latest Large Program (2011). We applied the two-sample Kolmogorov–Smirnov (K–S) test to the time series comparing the whole 2011 and 2006 profiles and the principal and secondary peaks individually, both for the whole energy band (0.15–3 keV) and the soft (0.15–0.3 keV) and hard (0.8–3.0 keV) ranges. Considering all of the above mentioned cases, the distribution functions of the two data sets resulted consistent, being the differences significant only at $\sim 2.3\sigma$. Moreover, we searched for possible spin phase shift or jumps among (and within) the two data sets (2006 and 2011) in order to check for possible long-term data acquisition system instability or irregular pulsar timing behavior. No significant phase shift was present when a planetary ephemeris was coherently used for solar system reference frame conversions. An upper limit of ∼0.04 (3σ) was computed by artificially introducing 100 phase shift trial values (step of 0.01) between the two time series before applying the K–S test. Obtaining instead barycentred times using ephemeris DE200 for the 2006s data set (the only available in the coeval SAS versions), and then using updated ephemeris DE405 for the new 2011s observation, one introduces an apparent phase shift of $\Delta\phi_{\rm spin} \simeq 0.07$ among the two data sets.

The possible temporal evolution of PSR A's pulse profile can also be evaluated, as a cross-check, considering the ratio of the two folded light curves normalized to their respective total counts. The result did not show any modulation, having a $\chi^2_{\rm red}$ significance value of $\sim 2.2\sigma$ ($\chi^2_{\rm red}$ applied to the ratio of the time series) and confirming the result obtained from the two-sample K–S test. Through the same technique, we estimated a phase shift between the two light curves of $0.008^{-0.006}_{+0.001}$ (errors at 1σ), slightly improving the upper limit obtained by the K–S test.

In summary, no significant pulse profile evolution or spin phase shift can be firmly claimed.

3.1. Pulse Phasing of PSR J0737−3039A

In order to better constrain the possible emission mechanisms providing the observed pulsed profile of PSR A, it is important to assess the relative multi-wavelength phasing of the pulsed peaks. This will also help us to further constrain the geometry of the system. Previous works studying the polarization of the radio profile (Demorest et al. 2004) showed that a possible interpretation of the double peaked pulsed profile is emission from a single big hollow cone of a nearly aligned rotator. On the other hand, Ferdman et al. (2013) suggested a double cone emission from an orthogonal rotator. In 2007, Chatterjee et al. compared X-ray and radio pulsed profiles, while Guillemot et al. (2013) compared radio and γ-ray ones. In this work, we collected the three profiles finding an X-ray/radio phasing in contrast with previous results.

Figure 2 shows the X-ray folded light curve in the 0.15–3.0 keV energy band, the 820 MHz radio profile obtained from GBT data with 64 MHz of bandwidth at epoch 55855 MJD, and the location of the peak maxima of the γ-ray profile produced with Fermi LAT data at energy $\geqslant$0.1 GeV (Guillemot et al. 2013). We determined that the maximum of the lower radio peak is located at phase 0.36 and the highest X-ray one is at 0.38 with a phase difference of 0.02 ± 0.03, while the highest radio peak is at 0.92 and the lower X-ray one at 0.98 with a difference of 0.06 ± 0.03 (the phasing error being determined by the relatively low count statistics of the X-ray light curve).

Our phasing result is shifted by ∼0.5 with respect to that reported by Chatterjee et al. (2007) in which the two highest X-ray/radio peaks and the two lower were corresponding. Phase jumps or shift artifacts in the *XMM-Newton* data are excluded from the clear evidence of peak coherence on the very long data span involving multiple data sets at different epochs.

Furthermore, we found a separation between the two X-ray peaks of $\sim 0.6 \pm 0.03$ ($\sim 216^\circ \pm 11^\circ$), while Chatterjee et al.

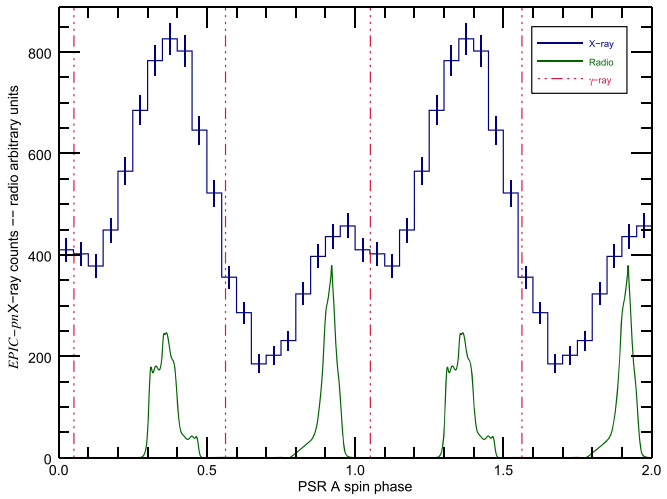

Figure 2. Result of phasing of the PSR A's pulsed profile. The X-ray profile obtained for 0.15–3.0 keV is represented by the solid blue line. The green line shows the radio profile at 820 MHz in arbitrary units. While the dotted–dashed red vertical lines indicate the phase value of the maximum of the γ-ray pulses. Two rotational phases are displayed for clarity.

(2007) reported an X-ray peak-to-peak separation of $\sim 182^\circ \pm 3^\circ$. In contrast with this latter result, the separation measured in this work is compatible (at least at the 2σ level) with the observed separation among the radio peaks ($\sim 200^\circ$; Manchester et al. 2005).

Our analyses suggest that X-ray and radio emission are coming from the same region of the magnetosphere (apparently unrelated to γ-rays) while the pattern of the radio emission (single or double cone) cannot be constrained by our result. We note that the absence of bridge emission in both radio and X-ray profiles is compatible with the hypothesis of a single hollow cone, in contrast with Chatterjee et al. (2007), a result that would imply a center-filled X-ray cone.

4. X-RAY EMISSION FROM PSR J0737−3039B

Evidence for pulsations ($\sim 4\sigma$) from PSR B in the 2006 *EPIC-pn* data set was obtained by Pellizzoni et al. (2008) for a (poorly constrained) orbital phase interval around the ascending node[12] of the pulsar's orbit.

In order to verify and better assess this detection, we first analyzed the new 2011 data alone and then reanalyzed 2006 data as a cross-check of previous results before proceeding with the comprehensive timing analysis of both data sets with a five-year gap.

PSR B's pulsed emission was investigated using the same period search method adopted for PSR A and radio ephemeris by Kramer et al. (2006). In this case, we could also use the lower time resolution *EPIC-MOS* data in addition to *EPIC-pn* data providing ~20,000 source counts overall (2006+2011 data sets), in principle, suitable for a timing analysis.

The search has been carried out using the Z_n^2 test (with n ranging from 1 to 5) accounting for detection parameters by Pellizzoni et al. (2008), both for the entire pulsar orbit and also focusing on selected orbital phase intervals (different longitude intervals w.r.t. ascending node). The best result of the search was obtained for $n = 4$ using a period search resolution of $\delta P = P^2/(n_{\rm bin} T_{\rm obs}) = 8 \times 10^{-7}$ s ($n_{\rm bin} = 20$) for the 2011 data. The Z_4^2 values resulting from 100 period trials around the radio period in the energy band 0.15–3.0 keV are plotted in the top left panel of Figure 3. The most significant spin period found in the search is 2.7734665(8) s (referred to the epoch 53156.0 MJD of the radio ephemeris) providing $Z_4^2 = 33.3$ and a $\sim 4\sigma$ confidence level (null hypothesis probability of 5×10^{-5}). The corresponding background-subtracted light curve is shown in the upper right panel of Figure 3. The χ^2 analysis applied to the same timing result indicates a $\chi^2_{\rm red} = 2.4$ (19 degrees of freedom, $\sim 3.5\sigma$). An even better detection significance is obtained applying the χ^2 statistics to a coarser binning (i.e., $\sim 4.2\sigma$ detection for $n_{\rm bin} = 10$). The pulsed flux in the 0.15–3.0 keV band is $\sim 1.4 \times 10^{-14}$ erg cm^{-2} s^{-1}, corresponding to a background-subtracted pulsed fraction of $\sim 16\% \pm 5\%$ ($n_{\rm bin} = 20$). The related X-ray luminosity is $\sim 1.6 \times 10^{29} \Omega_{\rm B}$ erg s^{-1} (where $\Omega_{\rm B} \sim$ 1–10 steradians is the pulsar beam solid angle), a value of the same order of the spin-down luminosity of PSR B.

In order to check the robustness of the detection of the relatively weak and peculiar signal from PSR B, we verified that our timing procedure was not affected by systematic errors artificially boosting χ^2 and Z_n^2 statistics. We replicated the timing procedure using fake radio ephemeris (randomly produced) and we verified that the occurrence of fake detection is compliant with the number of trials. For example, after $\sim 10^4$ random pulsar search trials, no fake detection $\geqslant 4\sigma$ in both χ^2 and Z^2 statistics was found.

Since the light curve of PSR A shows a larger unpulsed flux fraction in the soft energy band (0.15–0.5 keV), we verified that the detection significance of PSR B improves the restriction of the timing analysis in this band. The result shows a worsening of the signal in the 0.15–0.5 keV band, with a $Z_4^2 = 14$ ($\sim 1.8\sigma$). On the other hand, in the higher energy band (0.8–3.0 keV) the signal is still significant with a $Z_4^2 = 24$ ($\sim 3.1\sigma$).

We also carefully checked how detection significance changes, analyzing *EPIC-pn* and *EPIC-MOS* data separately. Both *EPIC-pn* and *EPIC-MOS* contribute to the detection of the pulsed signal from PSR B in the 0.15–3.0 keV band, though the significance of the *EPIC-pn* light curve is lower than expected ($\chi^2_{\rm red} = 1.6$) despite the fact that it yields about twice as many count statistics w.r.t. the *EPIC-MOS*. This can be explained by the fact that the *EPIC-pn* is much more affected by the strong and very soft background emission from PSR A. In fact, selecting higher energy ranges (e.g., 0.8–3.0 keV), the significance of the *EPIC-pn* light curve exceeds that of the *EPIC-MOS*.[13]

Periodicity was also investigated in four selected orbital intervals around conjunction and quadrature passages of the pulsar.[14] The light curves of PSR B obtained by folding *EPIC-pn* and *EPIC-MOS* counts in the selected orbital phase intervals —for the 0.15–3.0 keV energy band—are shown in Figure 4. Provided the low pulsed count statistics of the four orbital phase-resolved PSR B's light curves (Z_n^2 and χ^2 test

[12] I.e., orbital phase interval 0.38–0.63 assuming phase $\rm ph_A = 0$ as a reference for the passage of PSR A at the orbit's ascending node.

[13] The χ^2 statistic for $n_{\rm bin} = 10$ provides $\chi^2_{\rm red} = 2.0$ for the *EPIC-pn*, $\chi^2_{\rm red} = 1.8$ for the *EPIC-MOS,* and $\chi^2_{\rm red} = 3.4$ for the combined *EPIC-pn EPIC-MOS* light curves.

[14] Orbital phase intervals: *quadratures* [−0.125, 0.125] and [0.375, 0.625]; *conjunctions* [0.125, 0.375] and [0.625, 0.875] assuming phase $\rm ph_A = 0$ as a reference for the passage of PSR A at the orbit's ascending node and then $\rm ph_A \simeq 0.5$ for the same passage of PSR B.

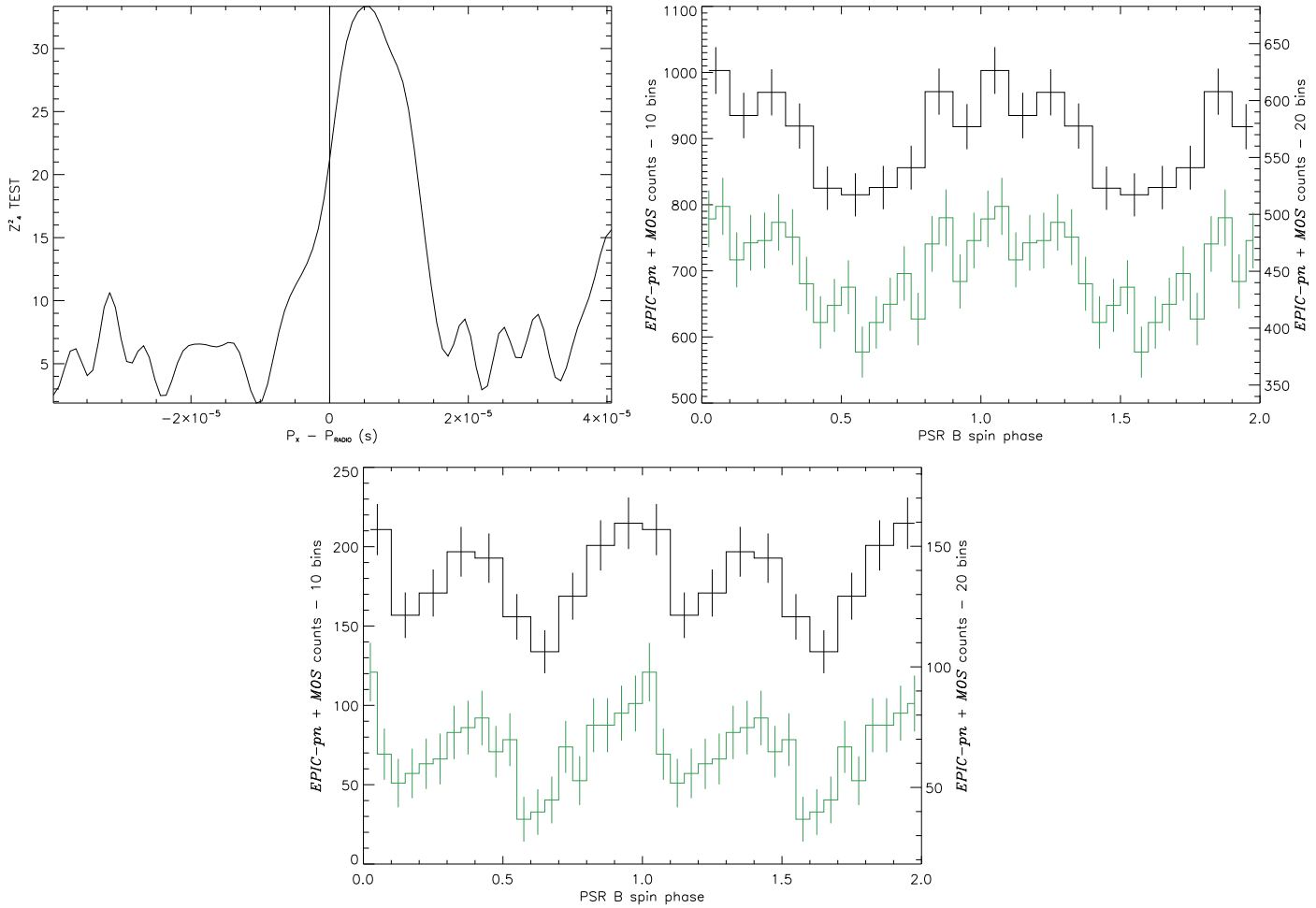

Figure 3. X-ray detection of PSR B. Top left: result of the Z_4^2 test distribution for 100 period search trials around PSR B's radio ephemeris. Top right: background-subtracted PSR B profile for the 0.15–3.0 keV energy band obtained by folding the 2011 combined *EPIC-MOS* and *EPIC-pn* data (both light curves with 10 bins—in black—and 20 bins—in green—are displayed). Bottom: same as top right, but selecting the orbital phase interval $\Delta\phi_{\rm orb} = 0.58$–$0.78$.

significance of the pulsed signal $\sim 1.8\sigma$ on average), variations of the pulse profile and pulsed fraction along the orbit cannot be firmly quantified.

After a blind search over a variety of orbital phase intervals (about 20 trials) selected spanning a range of widths and initial phase values, our most significant detection (with null hypothesis probability $\sim 10^{-2}$) is obtained in the range of 0.58–0.78. This result is shown in the bottom panel of Figure 3. The corresponding two-peaked light curve confirms changes in the pulse profile along the orbit or pulsar phase coherence loss (as also observed in the radio band by Burgay et al. 2003) maybe due to the peculiar process of illumination of PSR B and energy transfer from PSR A.

Moreover, the light curve of PSR B exhibits pulsed flux variations (>50%) along the orbit peaking in the orbital phase range $\mathrm{ph_A} = 0.65$–0.95 (see the pink region in Figure 4). Despite the fact that the significance of this result is $<2\sigma$ (likely due to the weakness of the signal from PSR B), we think that this issue is worth further investigation.

The measured X-ray period of PSR B differs by 5.7×10^{-6} s from the expected radio period at the same epoch ($P_{\rm B,radio} = 2.77346077007(8)$ s). Although the X-ray period search still yields a significant signal ($Z_4^2 \approx 22$), also at the nominal ephemeris value, the best X-ray pulse period that we find is significantly different from the radio one. Our high-precision timing results of PSR A fully exclude instrumental issues or other error sources in our timing procedure. On the other hand, we have to consider that PSR B's ephemeris errors obtained by Kramer et al. (2006) are only valid for the fitted time span of the radio observations due to the fragmented time interval in which PSR B is bright (see Kramer et al. 2006 for details). Nevertheless, this discrepancy among X-ray and radio timing of PSR B could have a physical origin. Recalling that PSR B disappeared in the radio band in 2008 and the radio ephemeris could not be updated since then, we cannot, in principle, exclude that glitches and/or significant timing noise occurred in the time between the radio and X-ray observations. Other viable interpretations should also be considered, e.g., the location of the emitting region far from the pulsar surface can affect barycentric corrections in the binary system. In fact, the period of PSR B detected by Pellizzoni et al. (2008) in the 2006 data set also presented a shift of $\sim 10^{-6}$ s with respect to the radio period. We verified the above result reanalyzing the 2006 data set through the new SAS version and updated the planetary ephemeris providing comparable results. We confirmed that in contrast with the 2011 observations, PSR B is not detected in the older data set when considering the whole orbit, nor when merging *EPIC-pn* and *EPIC-MOS* data, while the pulsed signal with the same features as in Pellizzoni et al. (2008) is found with a comparable significance analyzing

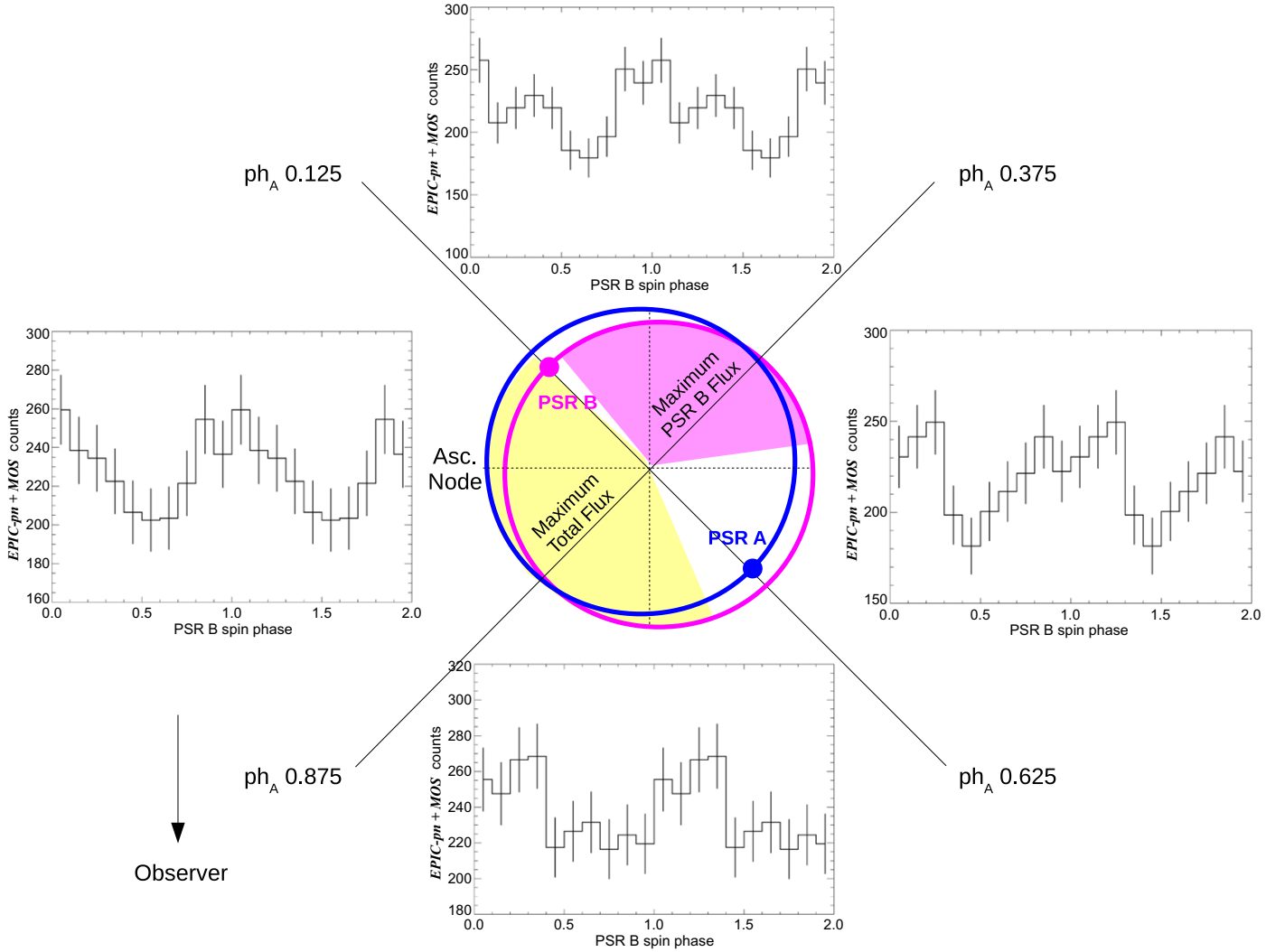

Figure 4. Central panel: scheme of the orbital configuration of PSR J0737−3039 in 2011 subdivided into four orbital phase intervals containing conjunctions ([0.125, 0.375]–[0.625, 0.875]) and quadratures ([0.875, 0.125]–[0.375, 0.625]). The yellow shaded region corresponds to the maximum of the total X-ray flux from the system (see Section 5 and Figure 5), while the pink area indicates the maximum of the PSR B pulsed flux (both shaded regions highlight the orbital phase intervals where PSR B is passing). The ph_A label in the figure highlights that phase 0 refers to the PSR A ascending node. The four plots displayed around the scheme show the PSR B (background-subtracted) pulse profile obtained by folding the 2011 *EPIC-MOS* and *EPIC-pn* counts belonging to the above mentioned orbital phases for the 0.15–3.0 keV energy band (the pulsed profiles are referred to as the orbital phase intervals where PSR B is passing).

EPIC-pn data in the orbital phase interval 0.38–0.63 (corresponding to the 0.41–0.66 in Pellizzoni et al. 2008). Pulse profile and spectral variations should then be invoked when comparing PSR B's peculiar behavior in the two different data spans at the two different epochs.

Finally, we repeated the above analysis for the entire *XMM-Newton* data set (2006+2011 data). Since among 2006 and 2011 observations the relativistic advance of periastron rotated the line of apsides by 84°.4, we shifted the binary phases of the second data set by this value to correct for the effect and effectively sum the counts arising from conjunctions and quadratures. Moreover, the relativistic spin precession produces a rotational phase shift, which would prevent coherent folding on such a large timescale. We then tried to recover the original phase, introducing arbitrary phase shifts in the light curve up to $\phi_{\rm spin}^{\rm max} \approx \Delta T_{\rm X}/P_{\rm prec} \approx 0.07$, where $\Delta T_{\rm X}$ is the time elapsed from the beginning of the 2006 observation and $P_{\rm prec}$ is the relativistic spin precession period (71 years; Lyne et al. 2004). The result did not show any modulation of the signal. The light curve evinces an almost flat behavior at all orbital phases.

Moreover, merging the two data sets without introducing any orbital phase shift due to the advance of periastron (and then necessarily neglecting observer-related orbital variability), we also verified that no emission enhancement/decrease deriving from the periastron and apoastron passages is present.

The lack of detection in this search on the overall *XMM-Newton* data set could possibly be related to the fact that PSR B's ephemeris may not be valid over such a long time span, or to a loss of phase coherence related to PSR B's X-ray emission mechanism connected to the energy transfer from PSR A.

5. ORBITAL VARIABILITY

Due to the noticeable evidence of peculiar interactions among the two pulsars both in radio and X-ray, a careful search for orbital flux variability with the strongly improved count statistics with respect to previous works was a fundamental step

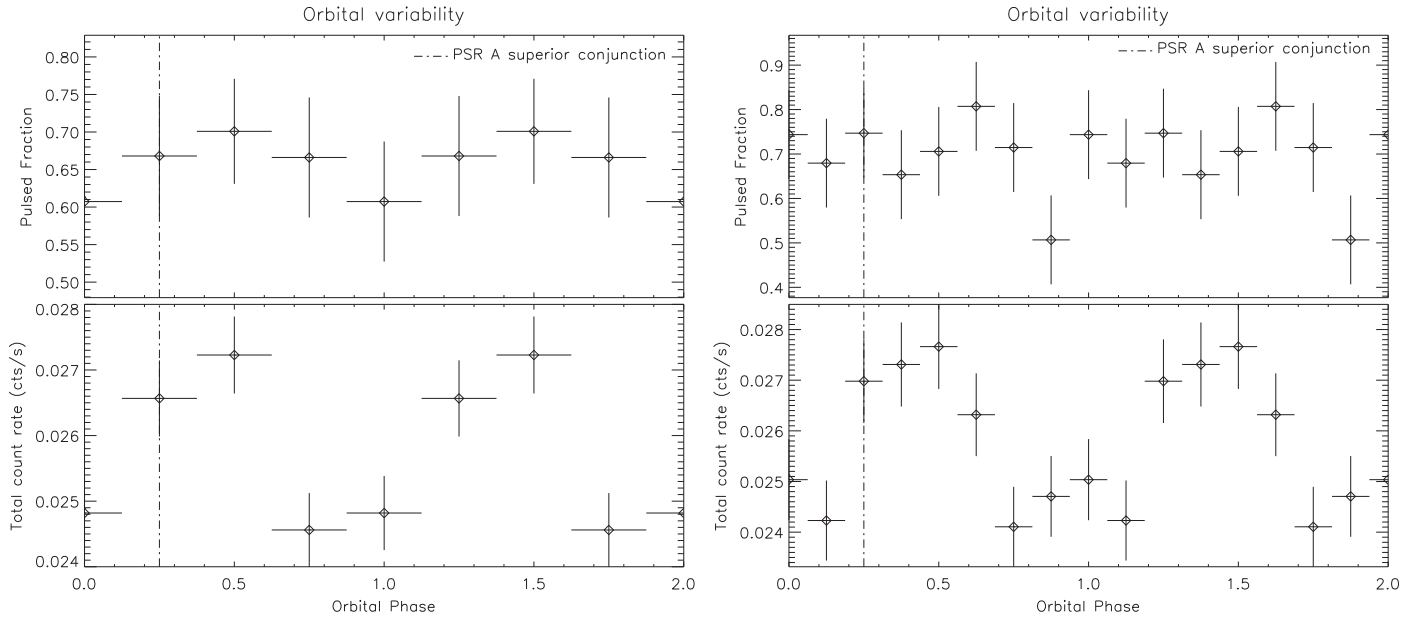

Figure 5. Background-subtracted pulsed fraction of PSR A (top panels) and orbital modulation of the total count rate from the system (bottom panels), in the 0.15–3.0 keV energy interval, obtained by folding ∼67 orbital periods (2006+2011 *EPIC-pn* data) and binning at ∼40 minutes (left) and ∼20 minutes (right). The vertical dotted–dashed line represents the superior conjunction of PSR A.

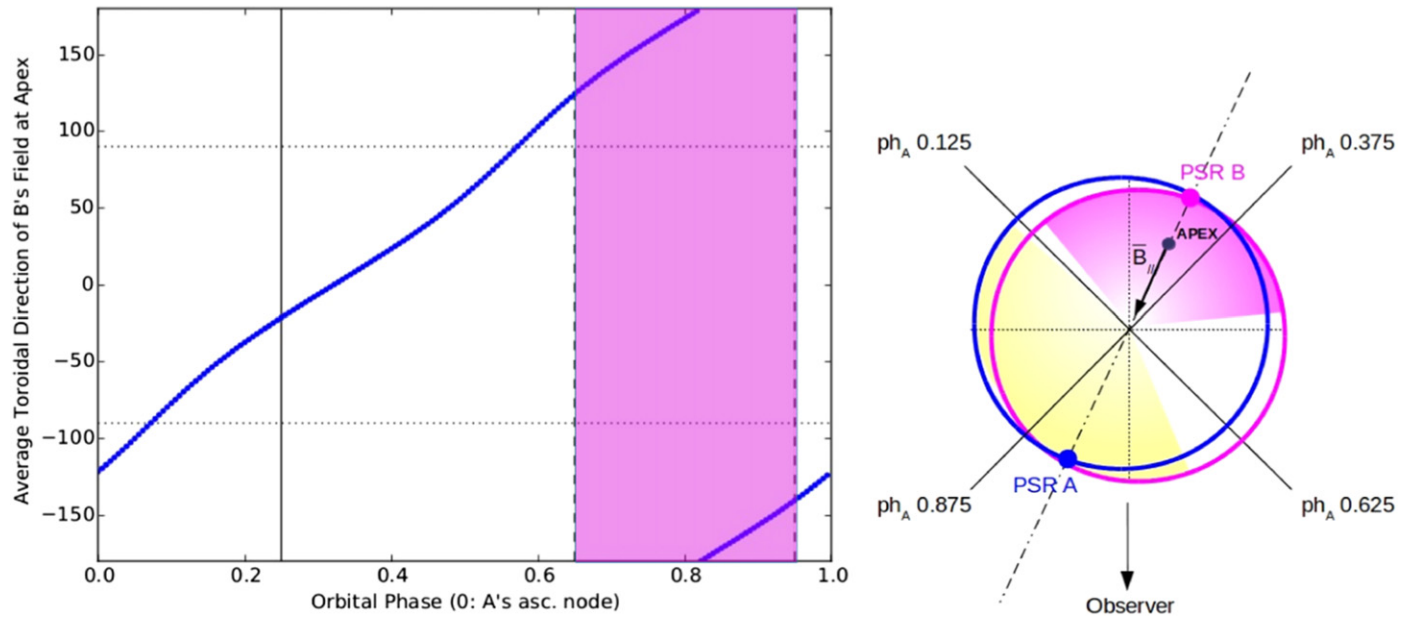

Figure 6. Left panel: component of the PSR B's magnetic field in the orbital plane averaged over one spin period. The pink shaded region indicates where the PSR B's flux reaches its maximum values, while the vertical black line marks the eclipse of PSR A. Right panel: scheme of the emission direction of PSR B. The black arrow at the top indicates the orientation of the average toroidal direction of the PSR B's magnetic field, $\overline{B}_{\parallel}$, when PSR B is located at the center of its brightest orbital phase interval, indicated by the pink shaded region. While the shaded yellow region represents the range of orbital phases in which the total flux reaches its maximum values.

in the system's timing analysis. Even though Pellizzoni et al. (2008) reported a quite stringent upper limit (<10%) on orbital flux variability, the X-ray emission of PSR B could possibly be associated with appreciable flux variation as a function of the orbital phase. Moreover, anisotropic high-energy emission could be produced at the interacting layer between PSR A's wind and PSR B's magnetosphere (see, e.g., Lyutikov 2005, bow-shock model). The bottom panels of Figure 5 show the background-subtracted orbital light curves obtained by folding ∼67 PSR J0737−3039 orbits in the energy band 0.15–3.0 keV, together with the corresponding pulsed fraction of PSR A (2006+2011 *EPIC-pn* data) shown in the top panels. Evidence of moderate orbital modulation of the total count rate is obtained when considering the entire *XMM-Newton* data set (bottom panels of Figure 5), while no significant detection of variability can be claimed from the analysis of the 2006 or 2011 data set separately. The full data set was processed taking into account the effects of the advance of the periastron, which occurred between the two observation periods (2006 and 2011) and correcting for their relative orbital phase shift, as we carried out PSR B's timing analysis. The analysis of modulation resulted in a $\chi^2_{\rm red} = 3.2$, with a null hypothesis probability

of 0.3% (~3σ) adopting an ~20 minute binning, and $\chi^2_{\rm red} = 5.2$, with a null hypothesis probability of 0.01% (~3.2σ) for an ~40 minute binning. The Z^2_n-test applied to the light curve provided a detection significance of 3.6σ ($Z^2_1 = 16$). The detection significance slightly improves when considering only the softer energy band (0.15–0.5 keV). The inclusion of *EPIC-MOS* data in the total flux variability analysis does not change the overall result.

The orbital count rate is clearly higher in the orbital phase range of ~0.2–0.6 (phase = 0 corresponds to the passage of PSR A at the ascending node) peaking at phase ~0.5, near the descending node of PSR A. The minimum of the orbital emission is at ~0.75, close to PSR B's superior conjunction. We observe approximately the same behavior in the soft (0.15–0.5 keV) and the hard (0.8–3.0 keV) energy bands. The total count rate variability fraction[15] is of ~(7 ± 1)%.

No significant orbital variability of PSR A's pulsed fraction (or correlation with flux variability) is evident above an upper limit of ~15% on the full energy band and also in the soft and hard sub-bands.

We noticed that the orbital phases corresponding to the maximum of the PSR B's pulsed flux do not correlate with the phases related to the maximum of the orbital flux (see Figure 4).

In order to probe possible effects due to intrinsic changes in the binary system (i.e., not related to the observer's line of sight), data were also inspected accounting for the possibility that the emission could rise around periastron epochs due to hypothetical pulsar interactions strengthening. In this case, no appreciable orbital flux variability was detected.

Since radio observations reveal a ~30 s eclipse of PSR A caused by PSR B's magnetosphere around PSR A's superior conjunction (orbital phase $\rm ph_A \simeq 0.25$), we also searched for possible X-ray variability on such a short timescale. Given the very high count statistics available, we calculated that a full ~30 s gap in X-ray PSR A flux should be, in principle, detectable at a >3σ level if present (~20–30 source counts missed). No signs of eclipse were found on light curves around PSR A's superior conjunction.

6. DISCUSSION

The Double Pulsar is a very complex source of X-ray emission arising from both neutron stars (including magnetospheric and possibly surface pulsed emission) and their peculiar interactions. *XMM-Newton* provided ~20,000 X-ray counts overall from the system obtained in the two data sets (~590 ks of observing time) separated by a five-year gap. During this period, PSR B disappeared in radio.

Our X-ray timing solution for PSR A obtained over a five-year data span represents the most accurate pulsar timing measurement performed by *XMM-Newton* so far, proving phase coherence stability of *EPIC-pn* time series on very long timescales. Martin-Carrillo et al. (2012) provided a systematic check of *XMM-Newton* timing calibration and performances based on long-term X-ray and radio pulsar monitoring. They defined the *relative timing accuracy* of an observation as the difference between the period measured with *XMM-Newton* and the period measured at radio wavelengths evaluated at the epoch of the X-ray observations. This difference was normalized to the pulse period measured in radio (see Equation (1) in Martin-Carrillo et al. 2012). The relative timing accuracy of *XMM-Newton* was proven to be better than 10^{-8} on average in their analysis. Applying the same method to our timing results on PSR A, we found a relative timing accuracy of ~10^{-12}, two orders of magnitude smaller than the smallest value found by Martin-Carrillo et al. (2012).

A detailed study of the radio pulse profile evolution of PSR B revealed that the relativistic spin precession was the cause of the radio emission disappearance with respect to our line of sight (Perera et al. 2010), which was observed in 2008. Although the spin precession rates of PSR A and PSR B are comparable, there is no evidence for secular variation in the radio pulse profile of PSR A (Manchester et al. 2005; Ferdman et al. 2008, 2013). Results of the visual inspection of PSR A's 2006 and 2011 X-ray light curves and K–S test (see Section 3) confirm this behavior endorsing that PSR A does not show clear evidence of precession likely because its spin misalignment from the orbital normal is very small. Relativistic spin precession of PSR A should also produce a relative spin phase shift between the 2006 and 2011 light curves of $\phi \approx \Delta T_{\rm X}/P_{\rm prec}\,\delta_{\rm A}$ for nearly aligned spin-orbit axes, where $\Delta T_{\rm X}$ is the time between the two observations, $P_{\rm prec}$ is the relativistic spin precession period, and $\delta_{\rm A}$ is the angle between the spin and the orbital angular momentum axes. We noticed that the phase shift minimizing the χ^2 of the ratio between the 2006 and 2011 folded light curves is $\phi \approx 0.008^{+0.001}_{-0.006}$ (1σ errors) corresponding to $\delta_{\rm A} \approx 6\overset{\circ}{.}6^{+1\overset{\circ}{.}3}_{-5\overset{\circ}{.}4}$, consistent with the value obtained by Ferdman et al. (2013).

From timing analysis, we assessed that ~16% of the source flux is provided by PSR B's pulsed emission, confirming the detection of the pulsar in X-ray even after its radio disappearance in radio in 2008. The peculiar phenomenology of PSR B and its weak flux required very careful cross-checks for detection verification.

PSR B is clearly detected folding the full 2011 data set in the 0.15–3 keV energy range, although it shows both pulsed flux and profile variations along the binary orbit possibly including slight spin phase shifts. This very unusual phenomenology is probably due to the peculiar X-ray brightening process of PSR B through energy transfer from PSR A and provides interesting clues about the complex pulsar interactions, but prevents the possibility to coherently fold the data over the entire *XMM-Newton* data span.

Discrepancy between the X-ray ($P_{\rm B,X} = 2.7734665(8)$ s) and radio ($P_{\rm B,radio} = 2.77346077007(8)$ s) periods of PSR B may arise from the time limited validity of radio ephemeris (Kramer et al. 2006). Alternatively, that could be ascribed to a physical origin. Changes in rotational parameters could, in principle, be possible as PSR B disappeared in 2008 and we are not able to witness the radio evolution of the pulsar. Glitches and/or timing noise could have occurred in the time between the radio and the second *XMM-Newton* Large Program. An alternative explanation is that the X-ray emission region could be located far from the neutron star surface, affecting the binary orbit timing corrections. Considering that the light cylinder of PSR B is approximately one-third of the neutron star's separation, if the emission region were placed in the outer part of the magnetosphere, it is clear that binary timing correction should be strongly affected: a smearing effect on the light curve up to 0.5–1 s (0.2–0.3 in phase) is expected as a function of the

[15] The count rate variability fraction is defined as $(C_{\rm max} - C_{\rm min})/(C_{\rm max} + C_{\rm min})$, where $C_{\rm min}$ and $C_{\rm max}$ are the minimum and the maximum count rates of the light curve respectively.

orbital phase. Moreover, the X-ray luminosity of PSR B is comparable with its spin-down energy, confirming that its brightening is due to PSR A energy injection.

The complex modeling of the orbit of this emitting region could, in principle, allow us to perform binary timing corrections with better accuracy improving the understanding and significance of pulsed signal from PSR B. The timing solution described in this paper could be used to search for the peculiar PSR B's pulsed signal in radio archival data arising from that region (even after its radio disappearance according to standard radio ephemeris). Also they will be valuable for studying the eclipse phenomenology.

The analysis of the full *XMM-Newton* data set provided evidence for the first time of flux orbital variability (~7% modulation amplitude). The observed count excess does not correlate with pulsed flux variations from PSR A nor from PSR B. The observed feature is likely associated with an additional emission component originating from an interaction layer between the neutron stars.

We expect that orbital-dependent persistent X-ray emission comes from the interaction of PSR A's wind with PSR B's magnetosphere (Lyutikov 2004). PSR B intersects approximately 0.01 of the PSR A wind, thus, we expect that the persistent X-ray emission would be <0.01 $L_{\rm A} \sim 6 \times 10^{31}\,{\rm erg\,s^{-1}}$, consistent with observations. The X-ray emission from the shock of PSR A's wind is expected to be orbital-dependent, since at different orbital phases the shape of the shocked layer of PSR A's wind at PSR B's magnetosphere (the magnetosheath) varies, approximately by ~15%. In addition, the velocities of the shocked plasma within the magnetosheath are mildly relativistic—this will tend to increase the modulation.

The pulsed X-ray emission from PSR B is the most puzzling. We suggest that in addition to a possible smearing on the light curve of PSR B caused by the altitude of the emission region (affecting the binary timing correction), high timing noise is present. This is due both to the orbital variations of the wind-magnetosphere interaction and the resulting turbulence in the magnetosheath. Some of the timing noise may, in fact, be non-random. Lomiashvili & Lyutikov (2014) reproduced many features of the orbital variation of PSR B radio emission, like the orbital variations of intensity, secular evolution of the radio profile, and the subpulse drift (McLaughlin et al. 2004b), by modeling the distortions of the magnetosphere of PSR B by the magnetized wind from PSR A. If the X-ray emission from PSR B is produced at high altitudes from the neutron star (see below), we expect variations of X-ray intensity. We suggest that it is related to synchrotron emission of particles from PSR A's wind trapped in the magnetosphere of PSR B (similar to van Allen belts in the Earth magnetosphere). The model of radio eclipses of PSR A (Lyutikov & Thompson 2005) requires a population of relativistic particles on closed field lines of PSR B.[16]

Let us estimate the expected synchrotron luminosity from the magnetosphere of PSR B. Synchrotron emission can be produced by particles only outside the cooling radius, where cyclotron decay time $\tau_{\rm c} \sim m_{\rm e}^3 c^5/(B^2 e^4)$ (with c the light velocity, B the magnetic field, and e and $m_{\rm e}$ the electron charge and mass, respectively) is of the order of the pulsar period,

$$r_{\rm c} \sim \left(\frac{B_{\rm NS}^2 e^4}{m_e^3 c^5 \Omega_{\rm NS}}\right)^{1/6} R_{\rm NS} = 2 \times 10^8\,{\rm cm} \quad (1)$$

where $B_{\rm NS} = 4 \times 10^{11}\,{\rm G}$ is the surface magnetic field of PSR B (Lyutikov 2004), $R_{\rm NS\ is}$ its radius, and $\Omega_{\rm NS}$ is the angular velocity. The synchrotron photon energy emitted at that radius is

$$\epsilon = \hbar \frac{eB(r_{\rm c})}{m_{\rm e} c} \gamma^2 = 10^3 \gamma_3^2\,{\rm eV} \quad (2)$$

where $\gamma_3 = \gamma/10^3$ is the Lorentz factor of emitting particles.

The emitting power from the whole magnetosphere can then be estimated as

$$L_X \sim \frac{4\pi}{3} r_{\rm c}^3 \frac{e^2}{c} \Omega_{\rm NS} B(r_{\rm c})^3 \gamma^2 n \sim \lambda B_{\rm NS} R_{\rm NS}^3 \gamma^2 m_{\rm e} c \Omega_{\rm NS}^2 \sim 2 \times 10^{31} \lambda_3\,{\rm erg\,s^{-1}} \quad (3)$$

where $\lambda_3 = \lambda/10^3$ parametrizes the density of emitting electrons with respect to Goldreich and Julian density at $r_{\rm c}$, $n \sim \lambda \Omega_{\rm NS} B(r_{\rm c})/(2\pi e c)$. We estimated $\lambda \sim 10^3$; large multiplicities are required by the eclipse modeling (Lyutikov & Thompson 2005; Breton et al. 2012).

The orbital dependence of the pulsed X-ray emission from PSR B may be due to reconnection-induced, orbital phase-dependent penetration of the wind plasma into PSR B's closed field lines. In the case of planetary magnetospheres, the plasma entry through the cusp[17] depends on the average angle between the cusp normal and the wind (Kallenrode 2004); in the Double Pulsar system, this average angle depends on the orbital location. We calculated the average (over one spin period) toroidal direction of PSR B's magnetic field component, $\overline{B}_{\parallel}$, as a function of the orbital phase, where toroidal here refers to the component of the field along the orbital plane of the system. The angle was calculated at the apex of PSR B's magnetosphere, i.e., at its magnetopause boundary along the line connecting it to PSR A. A toroidal angle of 0° indicates that $\overline{B}_{\parallel}$ is pointing away from PSR A on the line connecting it to PSR B, 180° is toward PSR A, 90° is parallel to the orbital motion, and −90° is anti-parallel. The result is displayed in the left panel of Figure 6, where the vertical black line marks the eclipse of PSR A and the pink shaded region is where PSR B is found to be brightest in X-rays. From what is shown in the plot, we can infer that PSR B's brightest phase is centered almost exactly around a toroidal angle of 180°, where $\overline{B}_{\parallel}$ is pointing toward PSR A and thus allows particles from the magnetosheath to penetrate more easily into the cusp.[18] This outcome strongly supports what we obtained from the observations and it can be visualized as the right panel of Figure 6.

7. CONCLUSIONS

In order to disentangle the X-ray emission from the two neutron stars and their interactions, the *XMM-Newton* data collected through two Large Programs on the Double Pulsar

[16] Plasma density and typical Lorentz factors of plasma particles cannot be determined independently, since the requirement of sufficiently high optical depth through magnetosphere put a constraint on the product $n\gamma^{-5/3}$, but not the n and γ independently.

[17] The cusp field line separates the field lines that close in the *head* and *tail* regions of the magnetosphere.

[18] Being toroidal angle 0° disfavored since reconnection (flux transfer events) requires an oppositely directed field.

require a careful step-by-step approach ranging from relativistic timing analysis to orbital/spin phase-resolved spectral analysis.

In this first paper, we presented detailed results on the long-term monitoring of PSR J0737−3039 allowing us to investigate about ∼80% of the binary system's total X-ray flux through an accurate timing analysis (i.e., from the total count, 60% and 16% are PSR A and PSR B's pulsed emission, respectively, and 7% is orbital variability). *XMM-Newton* demonstrated reliable and unprecedent millisecond timing capabilities over a five-year time span, providing for the first time physical constraints on PSR A's light-curve stability in X-ray and evidence for orbital flux variability likely associated with the interaction layer between the pulsars. We also provided evidences of X-ray pulsations from PSR B even after its radio disappearance. This peculiar phenomenology of PSR B can be ascribed to the particular location of the X-ray emitting region being different from the radio sites, and possibly situated far from the neutron star surface. We demonstrated that the enhanced emission occurs when the average toroidal component of PSR B's magnetic field is pointing toward PSR A, which implies that the inflow of new plasma is facilitated.

Relative X-ray flux contributions associated with the above findings provide the first set of inputs for a comprehensive and evolutive theoretical modeling of the system in X-ray, and offer a useful basis to proceed with spectral analysis and its correlation with timing analysis outcomes (E. Egron et al. 2016, in preparation).

Further monitoring of PSR J0737−3039 would be suitable for the *NuSTAR* X-ray mission over a few-year interval in order to confirm and study the evolution of *XMM-Newton* findings. *NuSTAR* could explore energies >6 keV with over an order of magnitude improved sensitivity with respect to *XMM-Newton* looking for pulsars interaction signatures free from strong pulsed soft emission and thermal components.

We thank S. Chatterjee for his helpfulness in cross-checking the PSR A's multiwavelenght phasing. This work is based on observations obtained using *XMM-Newton*, an ESA science mission with instruments and contributions directly funded by ESA member states and NASA. Alberto Pellizzoni, Elise Egron, Andrea Possenti, Sara Elisa Motta, Andrea Tiengo, and Marta Burgay acknowledge financial support from the Autonomous Region of Sardinia through a research grant under the programme CRP-25399 PO Sardegna FSE 2007-2013, L.R. 7/2007, *Promoting scientific research and innovation technology in Sardinia*. The research leading to these results has received funding from the European Union Seventh Framework Programme under grant agreement PIIF-GA-2012-332393.

REFERENCES

Arons, J., Backer, D. C., Spitkovsky, A., & Kaspi, V. M. 2005, in ASP Conf. Ser. 328, Binary Radio Pulsars, ed. F. A. Rasio, & I. H. Stairs (San Francisco, CA: ASP), 95
Becker, W., & Trümper, J. 1999, A&A, 341, 803
Blandford, R., & Teukolsky, S. A. 1976, ApJ, 205, 580
Breton, R. P., Kaspi, V. M., Kramer, M., et al. 2008, Sci, 321, 104
Breton, R. P., Kaspi, V. M., McLaughlin, M. A., et al. 2012, ApJ, 747, 89
Buccheri, R., Bennett, K., Bignami, G. F., et al. 1983, A&A, 128, 245
Burgay, M., D'Amico, N., Possenti, A., et al. 2003, Natur, 426, 531
Burgay, M., Possenti, A., Manchester, R. N., et al. 2005, ApJL, 624, L113
Campana, S., Possenti, A., & Burgay, M. 2004, ApJL, 613, L53
Chatterjee, S., Gaensler, B. M., Melatos, A., Brisken, W. F., & Stappers, B. W. 2007, ApJ, 670, 1301
Demorest, P., Ramachandran, R., Backer, D. C., et al. 2004, ApJL, 615, L137
Ferdman, R. D., Stairs, I. H., Kramer, M., et al. 2008, in AIP Conf. Proc. 983, 40 Years of Pulsars: Millisecond Pulsars, Magnetars and More (Melville, NY: AIP), 474
Ferdman, R. D., Stairs, I. H., Kramer, M., et al. 2013, ApJ, 767, 85
Guillemot, L., Kramer, M., Johnson, T. J., et al. 2013, ApJ, 768, 169
Kallenrode, M.-B. 2004, Space Physics: An Introduction to Plasmas and Particles in the Heliosphere and Magnetospheres (3rd ed.; Berlin: Springer)
Kalogera, V., Kim, C., Lorimer, D. R., et al. 2004, ApJL, 601, L179
Kramer, M., & Stairs, I. H. 2008, ARA&A, 46, 541
Kramer, M., Stairs, I. H., Manchester, R. N., et al. 2006, Sci, 314, 97
Kramer, M., & Wex, N. 2009, CQGra, 26, 073001
Lomiashvili, D., & Lyutikov, M. 2014, MNRAS, 441, 690
Lyne, A. G., Burgay, M., Kramer, M., et al. 2004, Sci, 303, 1153
Lyutikov, M. 2004, MNRAS, 353, 1095
Lyutikov, M. 2005, MNRAS, 362, 1078
Lyutikov, M., & Thompson, C. 2005, ApJ, 634, 1223
Manchester, R. N., Kramer, M., Possenti, A., et al. 2005, ApJL, 621, L49
Martin-Carrillo, A., Kirsch, M. G. F., Caballero, I., et al. 2012, A&A, 545, A126
McLaughlin, M. A., Camilo, F., Burgay, M., et al. 2004a, ApJL, 605, L41
McLaughlin, M. A., Kramer, M., Lyne, A. G., et al. 2004b, ApJL, 613, L57
McLaughlin, M. A., Lyne, A. G., Lorimer, D. R., et al. 2004c, ApJL, 616, L131
Pellizzoni, A., De Luca, A., Mereghetti, S., et al. 2004, ApJL, 612, L49
Pellizzoni, A., Tiengo, A., De Luca, A., Esposito, P., & Mereghetti, S. 2008, ApJ, 679, 664
Perera, B. B. P., McLaughlin, M. A., Kramer, M., et al. 2010, ApJ, 721, 1193
Possenti, A., Cerutti, R., Colpi, M., & Mereghetti, S. 2002, A&A, 387, 993
Possenti, A., Rea, N., McLaughlin, M. A., et al. 2008, ApJ, 680, 654
Ransom, S. M., Kaspi, V. M., Ramachandran, R., et al. 2004, ApJL, 609, L71
Strüder, L., Briel, U., Dennerl, K., et al. 2001, A&A, 365, L18
Turner, M. J. L., Reeves, J. N., Ponman, T. J., et al. 2001, A&A, 365, L110
Verbiest, J. P. W., Weisberg, J. M., Chael, A. A., Lee, K. J., & Lorimer, D. R. 2012, ApJ, 755, 39
Zhang, B., & Loeb, A. 2004, ApJL, 614, L53